energies

MDPI

Article

N Evolution and Physiochemical Structure Changes in Chars during Co-Pyrolysis: Effects of Abundance of Glucose in Fiberboard

Deliang Xu [1], Liu Yang [1], Ming Zhao [1], Yu Song [1], Karnowo [1,2], Hong Zhang [1], Xun Hu [3], Hongqi Sun [4] and Shu Zhang [1,*]

1 Joint International Research Laboratory of Biomass Energy and Materials, College of Materials Science and Engineering, Nanjing Forestry University, Nanjing 210037, China; xudl@njfu.edu.cn (D.X.); yangliu@njfu.edu.cn (L.Y.); zhaoming@njfu.edu.cn (M.Z.); song0105@njfu.edu.cn (Y.S.); karnowo@mail.unnes.ac.id (K.); zhanghong@njfu.edu.cn (H.Z.)
2 Faculty of Engineering, Universitas Negeri Semarang (UNNES), Jawa Tengah 50229, Indonesia
3 School of Material Science and Engineering, University of Jinan, Jinan 250022, China; xun.hu@outlook.com
4 School of Engineering, Edith Cowan University, 270 Joondalup Drive, Joondalup, WA 6027, Australia; h.sun@ecu.edu.au
* Correspondence: s.zhang@njfu.edu.cn; Tel.: +86-25-8542-8330

Received: 30 August 2020; Accepted: 25 September 2020; Published: 1 October 2020

Abstract: The simple incineration of wood-based panels (WBPs) waste generates a significant amount of NO_x, which has led to urgency in developing a new method for treating the N-containing biomass residues. This work aims to examine the N evolution and physiochemical structural changes during the co-pyrolysis of fiberboard and glucose, where the percentage of glucose in the feedstock was varied from 0% to 70%. It was found that N retention in chars was monotonically increased with increasing use of glucose, achieving ~60% N fixation when the glucose accounted for 70% in the mixture. Pyrrole-N (N-5) and Pyridine-N (N-6) were preferentially formed at high ratios of glucose to fiberboard. While the relevant importance of volatile–char interactions to N retention and transformation could be observed, the volatile–volatile reactions from the two feedstocks played a vital role in the increase in abundance of glucose. With the introduction of glucose, the porous structure and porosity in chars from the co-pyrolysis were dramatically altered, whereas the devolatilization of glucose tended to generate larger pores than the fiberboard. The insignificant changes in carbon structure of all chars revealed by Raman spectroscopy would practically allow us to apply the monosaccharides to the WBPs for regulating N evolution without concerns about its side effects for char carbon structures.

Keywords: nitrogen; evolution; co-pyrolysis; fiberboard; glucose

1. Introduction

The increase in demand for WBPs for furniture production has inevitably caused an increase in WBP-related residues; only in 2018, the worldwide production of WBPs was more than 400 Mm^3 [1], the disposal of which as waste has raised great concerns in terms of its environmental impact [2]. Since WBPs are mostly carbonaceous materials containing usually ~90% wood, combustion has been used as a convenient method for processing such bio-based residues into energy and/or heat for industry or households. However, WBPs have higher nitrogen content due to the inclusion of adhesive such as urea formaldehyde (UF) [3], which will cause server NO_x pollution if the WBPs residues are simply burnt in an incinerator. In comparison, pyrolysis, as another very common thermochemical conversion method for biomass, can effectively transfer WBPs into solid, liquid and gas products

under an inert reaction atmosphere [2]. The nitrogen-containing species derived from adhesive will also be distributed in the three-phase products at different extents and forms during the pyrolysis [4]. In gaseous products, NH_3 and HCN are the main species which are the key precursors of NO_x [5,6]. The amine-N and heterocyclic-N are found to be the key components in the pyrolytic liquid [7], which could be further refined as high-value products [8,9], such as catalysts [8–10], antibacterial agents [11] and so on. Meanwhile, the N-containing compounds are still problematic if the liquid is to be used as biofuel that will be eventually combusted in engines or turbines [12]. When the N is retained in the char, it endows the char with special functionalities and forms N-doped carbon materials as pollutant absorbents [13], electrochemical anodes [14], soil remediators [15] or catalysts [16]. Considering the renewable nature of biomass, the fixation of N in solid char could potentially achieve negative NO_x emission. Therefore, the effective regulation of N in char during pyrolysis of WBPs might offer an efficient kind of green treatment for WBPs-related residues [3] and simultaneously provide a feasible method to produce N-laden biomass-derived carbon [17].

Due to the importance of the fates and roles of N species, nitrogen transformation during the pyrolysis of biomass has been investigated extensively in recent years [18,19], especially in biomasses containing abundant N [20–22], such as, straws [23,24], algae [21], sewage sludge [25], pharmaceutical residues [26], shells of shellfish [27], WBPs [28] and other agricultural or food byproducts [23,29]. Besides the work focusing on the evolution mechanism of NO_x precursors [7,29–32], some other studies have explored stepped pyrolysis to reduce the release of NO_x. For example, Zheng et al. [33] torrified sewage sludge first and then conducted pyrolysis at 900 °C, showing that around 33% nitrogen could be removed by the first stage. Zhan et al. [34] and Girods et al. [35,36] managed to remove around 70% nitrogen from WBPs by low temperature pyrolysis (300–500 °C). Meanwhile, some works have tried to improve nitrogen content in biochar for preparing N-doped functional carbon materials [17]. For this purpose, two pathways have been considered. One is to use exogenous nitrogen as an N source, where biomass is pyrolyzed under NH_3 atmosphere [16,37] or by mixing with N rich species such as urea or melamine [38–40]. Secondly, as to the biomass with higher intrinsic N content, the key issue is how to maintain more nitrogen in char during pyrolysis. It was found that hydrothermal pretreatment could inhibit the release of nitrogen to a great extent [31]. Furthermore, co-pyrolysis between N-containing biomass and O rich biomass (such as saccharides) together could also significantly enhance the retention of N in the chars [41–43].

Sugars can react with amino acids or proteins to produce condensed and complex compositions through Maillard reactions, where N-containing groups can combine with O radicals actively [44]. The N-functional groups on char surfaces and in the gas phase could be then possibly captured by O-containing radicals during the pyrolysis reactions [45]. It has been reported that amide-N derived from UF can be decomposed into NH2- and -NH- that would react with –C=O [42,46] and then recombine back to biochar [17]. Based on this reaction mechanism, glucose was used as an agent blended with microalgae to conduct hydrothermal treatment, leading to an obvious improvement of N content in the derived carbon [43]. When conducting co-pyrolysis of glucose and fiberboard (FB), one of the most common WBPs, results also showed that the N fixation in chars could be doubled with 50 wt.% glucose blended in the feedstocks at temperatures from 300 to 700 °C [3]. Additionally, when conducting co-pyrolysis of bamboo and N rich microalgae, more nitrogen transforming into char has been found with increased proportions of bamboo. This may be also because of interactions between cellulose-derived saccharides and N species [41,47]. More fundamental works on co-pyrolysis of glucose and biomass containing abundant N would help to further explain the nitrogen transformation mechanism during the pyrolysis of N-laden lignocellulosic biomass. The insights into the fundamental reactions with N species would also shed light on the possibility of seeking more economical and sustainable substitutes for glucose from the biorefinery industry in the future.

So far, the effect of proportion of glucose in the feedstock on the N evolution and transformation still remains unclear. It is always desirable to have a minimal amount of glucose in WBPs to simplify the operation and reduce the cost. The change in the proportion of glucose in raw materials will

not only vary the N retention and chemical forms but also possibly impact the carbon structure of resultant chars, especially at the high concentrations of glucose that will be the dominant precursors for char formation. Although the distribution and types of N-containing groups are the main factors in determining the functional properties of N-doped carbon materials, the physiochemical structure of carbon supports can largely interact with the N species and thus affect its electrochemical and catalytic performance. Therefore, the purpose of this work is to investigate the effect of abundance of glucose in the feedstock on nitrogen retention and transformation during co-pyrolysis with fiberboard, and the changes in physicochemical properties of the chars were also examined. It has been found that the increase in the ratio of glucose to fiberboard has effectively enhanced the N retention while exerting little effects on the carbon structure in chars.

2. Materials and Methods

2.1. Materials

FB from Dare Technology Co., Ltd., Zhenjiang, China was used for the WBPs samples in this study. The nitrogen content of FB was 5.80 wt.% (db), which originated from the addition of melamine modified urea formaldehyde during the manufacture process. Glucose was purchased from Shanghai Aladdin Biochemical Technology Co., Ltd. FB was crushed firstly, and then sieved to 0.15–0.20 mm for use. Before pyrolysis experiments, FB powder was dried for around 12 h in an oven at 105 °C.

2.2. Pyrolysis in the Fixed-Bed Reactor

As is shown in Figure 1, the quartz tube reactor (870 mm × 40 mm) was fixed in an electrically heated furnace. Then, 3 g well-mixed FB and glucose at various ratios were preloaded onto the quartz frit in the middle of the tuber reactor. When conducting pyrolysis experiments, the sample was heated at 20 °C/min till the prescribed temperature of 500 °C was reached, with a holding time of 60 min; the whole process was controlled under Ar atmosphere. The volatiles flew through a U-type tube that was soaked in ice-water to be condensed. Before being released into the atmosphere, the flue gas was washed in a flask containing water. Char yields was obtained by measuring the weight difference in the reactor before and after pyrolysis experiments. The nitrogen contents in solid samples were detected by a Vario ELIII Elemental Analyzer (Elementar, Germany).

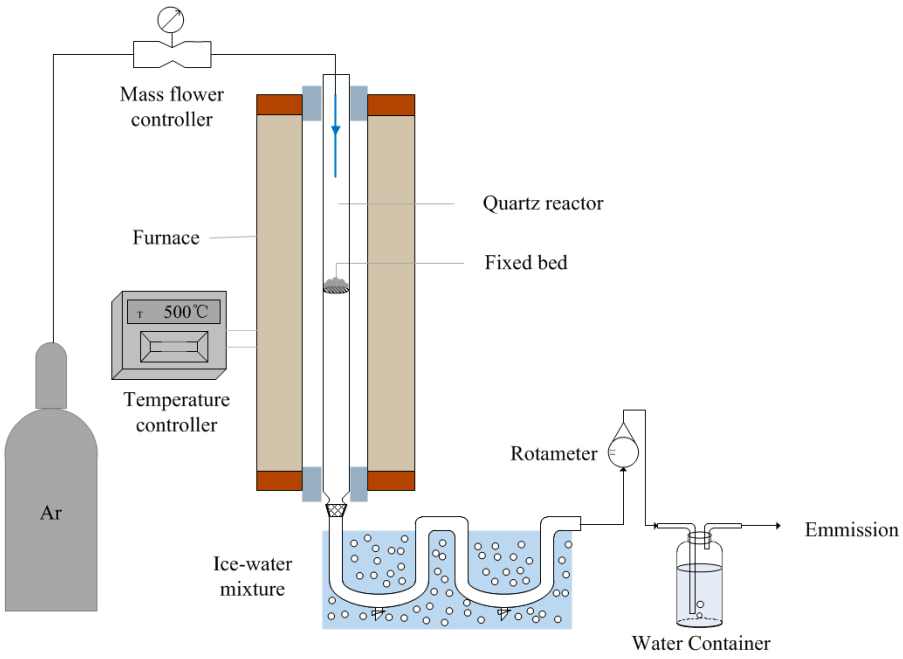

Figure 1. Schematic digram of the experimental set-up [3].

The retention of nitrogen in char was determined as follows:

$$\boldsymbol{N}_{rentention} = \frac{mass\ of\ nitrogen\ in\ char}{mass\ of\ nitrogen\ in\ raw\ material} = \frac{\boldsymbol{M}_{char} \times \boldsymbol{N}_{char}}{\boldsymbol{M}_{feedstock} \times \boldsymbol{N}_{feedstock}}$$

where $\boldsymbol{M}_{char}$—the mass of char, g; $\boldsymbol{N}_{char}$—the nitrogen content in char, wt.%; $\boldsymbol{M}_{feedstock}$—the mass of feedstock, g; $\boldsymbol{N}_{feedstock}$—the nitrogen content in feedstock, wt.%.

2.3. Characterization of N Functional Groups in Chars

Nitrogen-containing functional groups in chars were semi-quantified by X-ray photoelectron spectroscopy (XPS), and the proportion of a single peak area in the total peak areas was calculated and regarded as the relative content of the nitrogen functional group in char. AXIS Ultra DLD (Kratos, UK) was used to carry out detections; more information about the configuration, measuring settings and spectra analysis of XPS can be seen in our previous paper [3].

2.4. Measurements of Physiochemical Structures in Chars

N_2 adsorption/desorption isotherms were measured by an automatic surface area and pore analyzer (autosorb iQ, Quantachrome, Boynton Beach, FL, USA). All samples were degassed at 150 °C for 12 h and then adsorbed by N_2 at −196 °C. The surface area and pore size distribution were analyzed by the multipoint Brunauer–Emmett–Teller (BET) method and density functional theory (DFT) method, respectively.

The surface morphology of co-pyrolysis char was analyzed by scanning electron microscopy (SEM). Quanta 200 (FEI Co., Hillsboro, OR, USA) was used to obtain SEM photos; gold coating treatment for all samples was done by PECS (Gatan Inc., Pleasanton, CA, USA). In the scanning process, 20 kV voltage and vacuum environment were employed.

The carbon structures in chars from the co-pyrolysis were measured by a Raman spectrometer (LabRAM HR Evolution) from Horiba Ltd., Kyoto, Japan. The excitation laser wavelength was 532 nm and the laser power was 1 mW. The original Raman spectra were deconvoluted into 10 Gaussian bands, which has been detailed in previous studies [48–50]. Briefly, the D (1300 cm^{-1}) band reflects the carbon structure with no less than 6 aromatic fused aromatic rings, while G_R (1540 cm^{-1}), V_L (1465 cm^{-1}) and V_R (1380 cm^{-1}) bands together represent the smaller aromatic ring systems with 3–5 fused rings. Therefore, the ratio between D band area and (G_R + V_L + V_R) band area would mean the relative abundance of large aromatics in chars.

3. Results and Discussion

3.1. Effects of FB:Glucose Ratio on N Contents and Retention in Chars

As is shown in Figure 2, the significant increase in the proportion of glucose in the feedstock did not result in a considerable increase in char yields, although slight gains in char weight could be discernable when the ratio between FB and glucose was 3 to 7. The increase in percentage of glucose that contained no N must have proportionally decreased the total amount of N in the blended feedstock. Unexpectedly, the nitrogen contents in the resultant biochars did not reduce owing to the enhanced N fixation, which caused a linear increase in N retention in chars as a function of glucose percentage in feedstock. The N retention was calculated by the N in char over the N from feedstock.

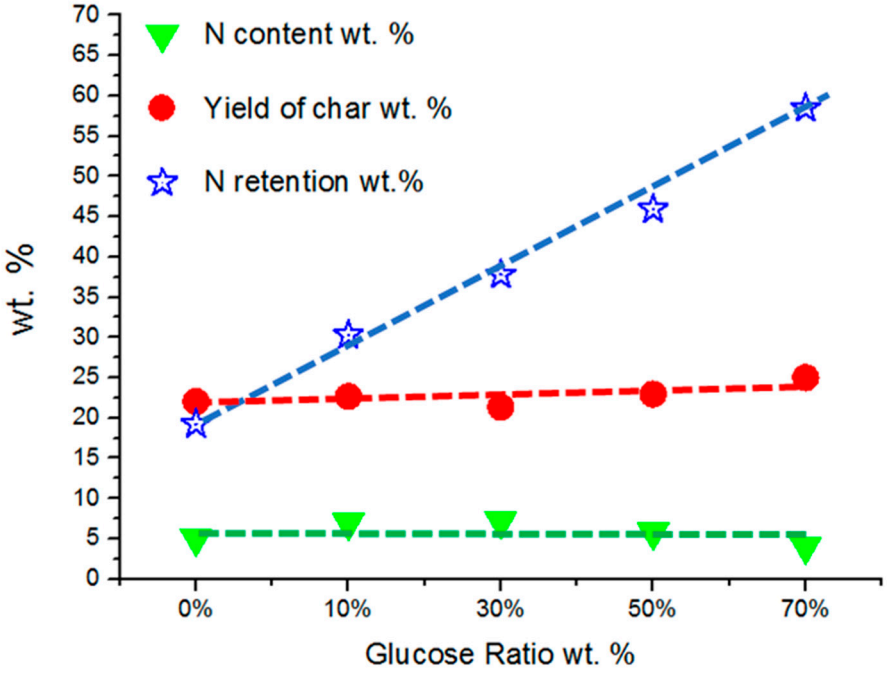

Figure 2. Nitrogen content, char yields and nitrogen retention as a function of glucose percentage in feedstock.

In the absence of glucose, the values of char yield were slightly lower than those of N retention, indicating that the decomposing extent of UF containing N species in the FB was somehow higher than wood substance at the reaction temperature of 500 °C, which was due to the labile nature of amide-N in UF at low temperatures [34,36]. With the addition of glucose into the FB, the char yields stayed nearly unchanged, while the N retention continued to increase with the increase in the percentage of glucose in the mixed feedstock. This means that the co-pyrolysis with glucose greatly facilitated the N transformation from volatile-N to char-N, which was probably due to the reactions between radicals (especially those active O-containing functional groups) derived from glucose and the decomposed N-species from FB [17], forming heterocyclic N-containing compounds and thus recombining back to chars [3]. It is also possible that the formation of glucose-derived liquid compounds featuring a caking property played a role in preventing the volatile-N from escaping the char particles. However, considering the significant increase in N retention from around 19% to 30% when only 10% glucose was present in the mixture, the mechanism of solid–solid interaction might be less important. Besides the volatile–volatile reactions, the abundant radicals from the decomposition of glucose may possibly stabilize the active sites, thus terminating the reactions responsible for the release of N species from FB. It is also interesting to note that the change in the proportion of glucose over the broad range could not apparently impact the N content, which was always at ~5%, suggesting that there might be a limitation for the N anchoring capacity by chars produced under the experimental conditions.

The positive relationship between the N retention and the percentage of glucose in the feedstock confirms that the concentration of glucose-derived volatiles was a critical factor in retaining N in chars. On the other hand, the increase in the use of glucose must have altered the secondary reactions to a certain extent [3,51]. For example, the volatiles from the primary decomposition of glucose may interact with wood-derived chars or volatiles before reacting with UF-derived N-containing species when the glucose is in a small proportion. When the glucose was dominant in the mixture, secondary reactions may likely occur among glucose-derived products. The linear increase in N retention with the increase in use of glucose implies that the various active compounds in the gas phase could be effective in the fixation of N in chars. The exact reaction mechanism related to the specific active species here remains unknown and further study is warranted.

3.2. Effects of FB:Glucose Ratio on N Transformations in Chars

XPS spectra of chars from the co-pyrolysis of FB and glucose at different ratios are shown in Figure 3. In carbonaceous material surfaces, five types of N-containing species, named pyridine-N, pyrrole-N, quaternary-N, pyridone-N and oxidized-N, could be formed as functional groups, depending on experimental conditions. As is shown in Figure 3a, only amide-N with the binding energy located at 399.8 eV could be identified from the fiberboard. The amide-N was mainly derived from UF resin, in which -NH-, C=O and -CH2- were the main composing units [52]. When examining the chars from co-pyrolysis of FB and FB-glucose at 500 °C, no peak at 399.8 eV could be seen in the spectra, indicating that all amide-N originally existing in FB disappeared due to the vulnerability of amide-N under the decomposing reactions [34,36]. Instead, three distinguished peaks located at around 398.6, 400.5 and 402 eV clearly emerged, corresponding to the assignments of pyridine-N, pyrrole-N and quaternary-N, respectively [7,17,53].

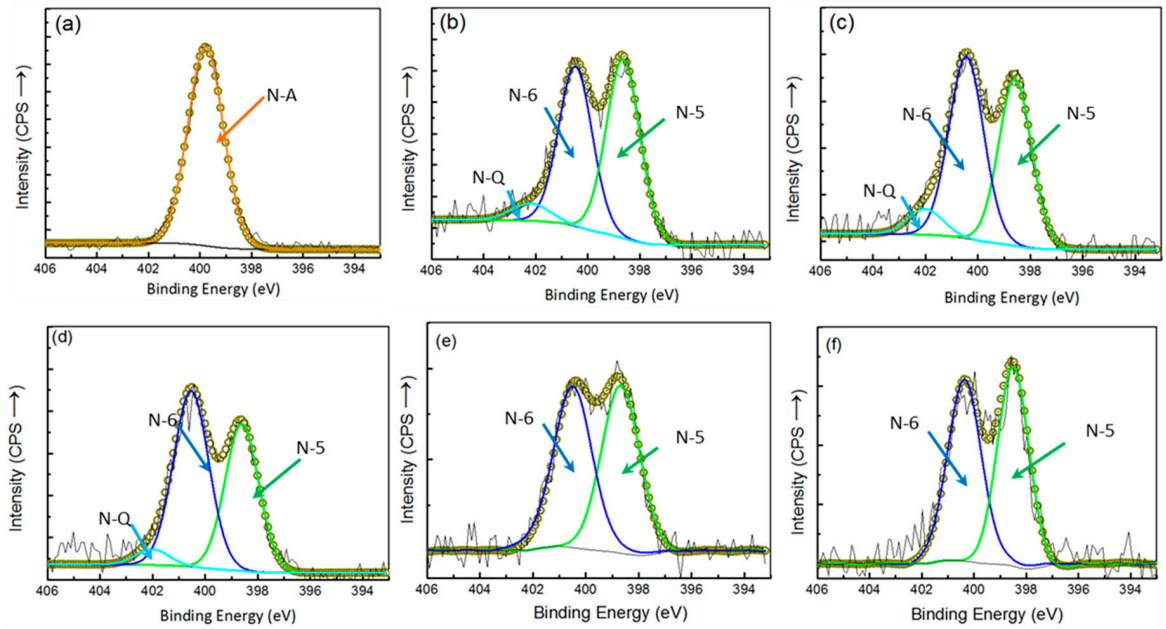

Figure 3. N 1s XPS spectra: (**a**) FB; (**b**) char from FB; (**c**) char from FB with 10% glucose; (**d**) char from FB with 30% glucose; (**e**) char from FB with 50% glucose; (**f**) char from FB with 70% glucose (N-A: Amide-N, N-5: Pyrrole-N, N-6: Pyridine -N, N-Q: Quaternary-N).

The relative contents of each N-functional group were calculated by taking the percentage of sub-peak area of each N-functional group in the total peak area as follows.

$$RC_{N^*} = \frac{A_{N*}}{\sum A_{N*}} \times 100\%$$

where RC_{N^*} refers to the relative content of each N-functional group, and A_{N*} means the sub-peak area of N-functional group.

Figure 4 shows the relative contents of N-functional groups distributed in the chars as a function of percentage of glucose in the blended feedstock. The most striking difference was that the N-Q could be obviously detected when the portion of glucose was lower than 50%, and it completely disappeared with the increase in glucose abundance up to 70%. The nitrogen atom of N-5 and N-6 appears at the edge of graphitic layer, while the N-Q is evolved when a carbon atom in the center of a graphitic layer is displaced by N. Usually, the N-5 and N-6 were firstly produced from the pyrolysis of amide, amino and protein N inside biomass. With temperature increasing to around 500 °C, a more stable structure of N-Q could be formed via cyclic condensation reactions from N-5 and N-6 [54,55].

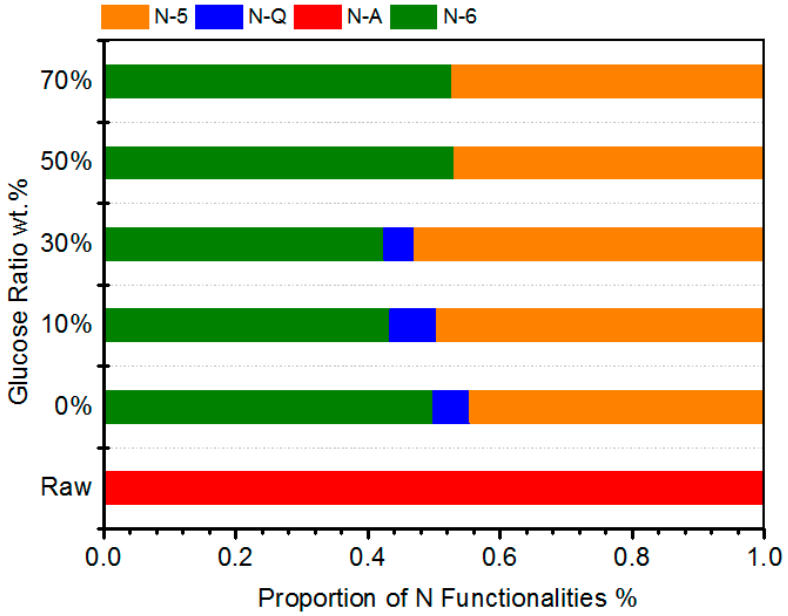

Figure 4. The relative content changes of nitrogen functionalities with different glucose ratios.

In this work, the transformation of N-functional groups in chars during the co-pyrolysis of WBPs and glucose may follow three possible reaction pathways. Firstly, at the low concentrations of glucose in the mixture, the amide-N in UF would decompose rather independently, and thus most N were released as amino groups in the gas phase. Meanwhile, the remaining N from the primary reaction would slowly transfer to N-5 and N-6 in char via dimerization and cyclization [7,34]. Secondly, the abundant nitrogen-containing groups generated from the deamination reactions of amide-N mainly presented as amino-N (NH2-, -NH-) in the volatiles [34], and nitrogen species in the gas phase had a strong intention to substitute for O atoms in the surface of char through Maillard reactions during the secondary reactions (volatile–char interactions) [3,17]. Particularly, the char derived from glucose contained fruitful O groups (OH-, C=O, etc.), which led to the high N retention in chars, as discussed above [17]. Thirdly, the initially escaped N species could be captured by the O-containing radicals due to the enhanced volatile–volatile reactions with increasing proportion of the glucose [12,34]. Therefore, the ultimate N retention in chars was as a result of three reaction pathways, where the N from the first two sources was directly bound to the char substrate, while the N from the third one was mainly formed in the gas phase. The char-originated N-5/6 could be further converted into N-Q by condensation reactions and N migrations inside the char matrix. On the contrary, the volatile-originated N-5/6 would mainly lie in the volatile-derived less fused carbon on the char surface and were thus reluctant to be transferred to N-Q, which might be the reason for the lack of N-Q observed when the percentage of glucose was high. It was also found in the literature that N-5/N-O instead of N-Q was mainly formed on the char surface with the enhancement of defected char structure by KOH addition [9]. N-5 showed an increasing tendency in char prior to 30% glucose used in the feedstock, which was followed by an increase in N-6 with increasing glucose till 70%. It appears that the Maillard reactions in the volatile phase preferred to produce N-containing six-membered polyaromatic structures.

3.3. Effects of FB:Glucose Ratio on Physiochemical Property in Chars

Besides the detailed examination of the N retention and transformation in chars from the co-pyrolysis of FB and glucose at various ratios, a strong emphasis was also placed on the possible changes in the physiochemical structure as the carbonaceous matrix of chars would inevitably affect the photoelectric properties of N-containing functional groups. As is shown in Figure 5a, the surface areas of the chars from co-pyrolysis obviously decreased, compared to those of char from FB only. It is

understandable that the recombination of solid coke/soot derived from the volatile–volatile interactions as mentioned above would lead to the sudden reduction in porous structure. With the increase in the proportion of glucose, the values of the surface area of chars gradually increased, reaching nearly 19 m^2/g for the char with 70% glucose in the mixture. Once the glucose becomes the dominant component during the co-pyrolysis, the resultant char mainly comes from the decomposition of glucose and the recombination due to the volatile–volatile reactions may become less significant. In addition to the variations in surface areas, the shift in pore size distribution (PSD) could be also clearly observed when increasing the percentage of glucose, as is shown in Figure 5b–f. It appears that the introduction of glucose intended to generate larger pores than that of FB did, which can be verified by the comparison between the one-peak and the two-peak spectra in the Figure 5b–f. Since FB comprises the UF and wood containing the three main components of hemicellulose, cellulose and lignin, the decomposing process started from the UF and hemicellulose at ~200 °C [3,28]. Therefore, the gradual devolatilization of various elements and the subsequent condensation reactions of lignin-derived compounds together caused the relatively small porous structure. The homogeneous nature of glucose would decompose at a narrow temperature zone, and more importantly, the decomposing reactions for the glucose particles must initiate from the surface due to the low heat transfer coefficients, which will likely create large pores in the glucose-derived chars. As a result, the selective decompositions at different heating stages in the case of FB were more likely to facilitate the formation of small pores with relatively high surface areas.

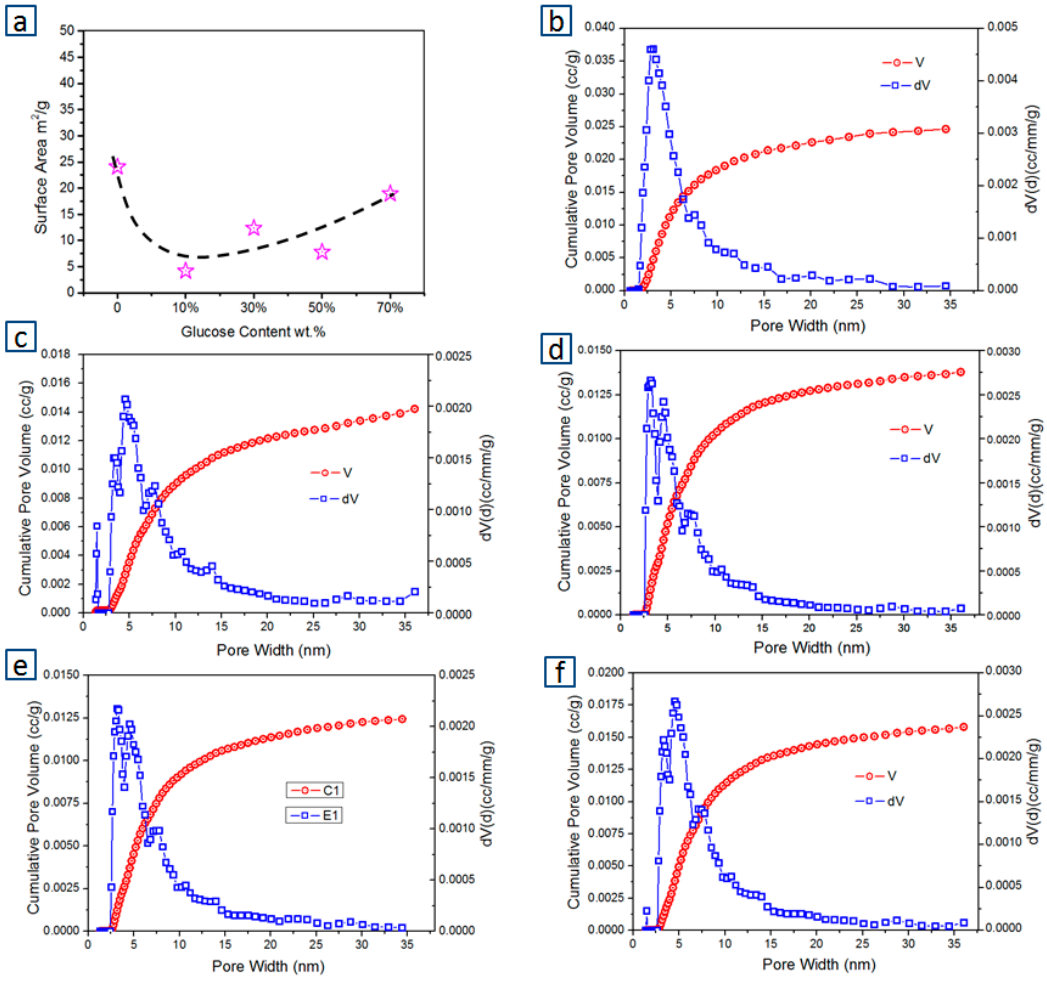

Figure 5. (**a**) Surface area in chars from different glucose: FB ratios; (**b**) pore size distribution (PSD) of char with no glucose; (**c**) PSD of char with 10% glucose; (**d**) PSD of char with 30% glucose; (**e**) PSD of char with 50% glucose; (**f**) PSD of char with 70% glucose.

The surface morphology was obtained by SEM analysis and was in direct agreement with the measurements of the porosity above. The FB power from the mechanical processing maintained its irregular and fibrous shapes [2,56], as shows in Figure 6a, where some of the woody fibers tended to agglomerate and form bundles in their shape. With a low proportion of glucose added into FB, the biochar morphology did not obviously change (see Figure 6b,c). With further increase in glucose from 30% to 70% in the feedstock, the agglomeration of resultant chars became more severe, among which nearly no single fibrous char particle could be observed in Figure 6f. At the same time, relatively large pores emerged with the increase in glucose content in the mixture, which is in good agreement with the pore size analysis by the BET method.

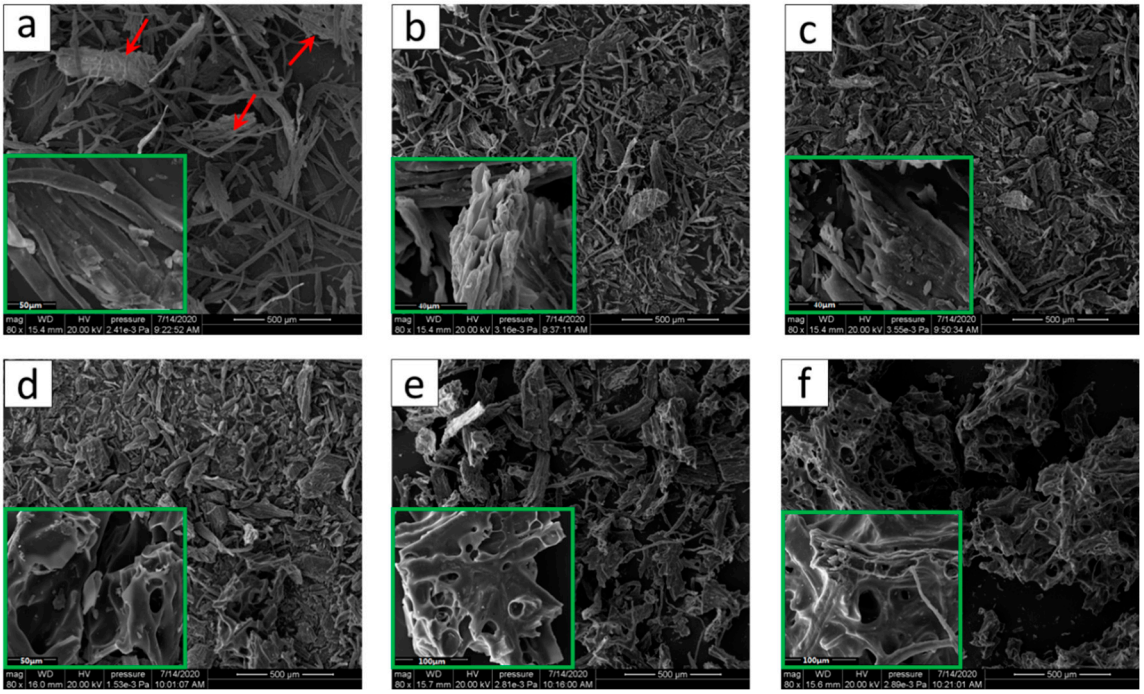

Figure 6. The morphology changes in chars from the co-pyrolysis of fiberboard and glucose at 500 °C: (**a**) FB; (**b**) char from FB; (**c**) char from FB with 10% glucose; (**d**) char from FB with 30% glucose; (**e**) char from FB with 50% glucose; (**f**) char from FB with 70% (the photos inside the green box show higher magnification).

The higher magnification images shown in the green box of Figure 6a–f were obtained to further probe into the effect of glucose on the morphology of char surface. Except the char derived from 10% glucose addition, the surfaces of chars derived from the feedstock containing higher ratio of glucose showed very clear molten phase deposition. The molten phase was formed from the glucose before carbonization [57]. The glucose-derived liquid phase led to the agglomeration of char particles and also increased the contact surface areas between char and volatiles. It is believed that the occurrence of the molten phase on the surface of FB char would delay the emission of N-containing groups and thus improve the N retention in the co-pyrolysis chars.

It has been widely recognized that chars originated from biomass at low to medium temperatures contain very limited crystalline carbon structures. Therefore, a Raman instead of X-ray diffractometer (XRD) has been employed to characterize the amorphous carbon skeleton structure in recent years. Generally, two broad peaks of G band at 1580–1600 cm^{-1} and D band at 1350–1370cm^{-1} will be obtained for almost all the biochars [58]. While the G band represents the graphitization degree of ordered carbon materials, it mainly reflects the quadrant ring breathing here from the amorphous biomass chars. As introduced in the experimental section, the combined peak areas of Gr, Vl and Vr could denote the abundance of the small aromatic ring system, whereas the signal of the D band was mainly

contributed by the large aromatic ring system (no less than six fused rings). The intensity ratio between $I_{(Gr+Vl+Vr)}$ and I_D could thus indicate the relative richness of the small aromatic ring system in the char matrix, giving a measure of the amorphous extent of chars [48,50]. As is shown in Figure 7, the values of $I_{(Gr+Vl+Vr)}/I_D$ did not see any apparent alteration with the increase in use of glucose in the feedstocks, suggesting that the carbon in the chars share similar structural characteristics regardless of the origins of solid carbons from the FB, the glucose or the soot/coke from the volatile–volatile and/or volatile–char interactions. The lowest impact of glucose addition on the char structure could be very favorable in terms of the potential applications of the N-containing functional carbon materials. In other words, when we examine the effects of glucose on the N retention and transformation during co-pyrolysis with FB, its side effects on the body carbon structure will be of little concern. This will further increase the practical feasibility of using monosaccharides as the promoters to convert waste FB into valuable carbon materials.

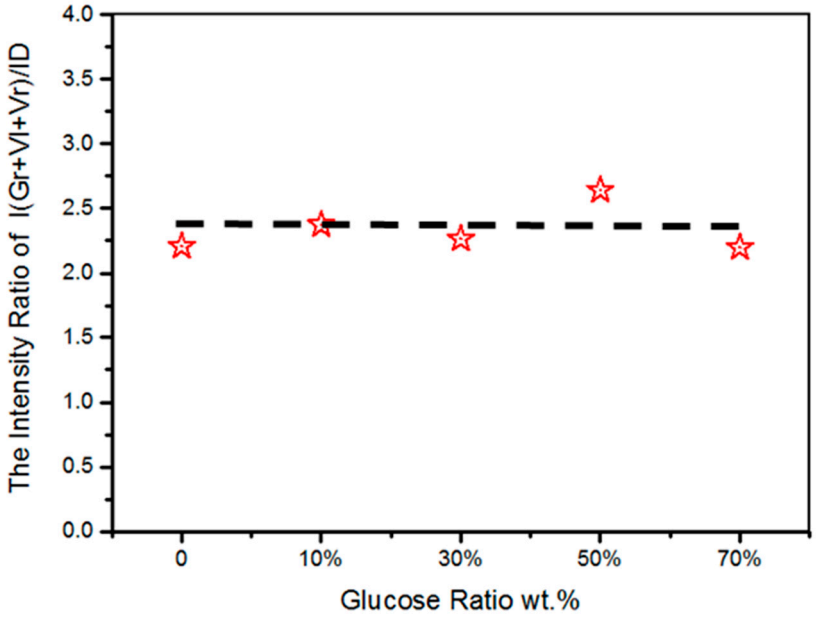

Figure 7. The changes in the ratio of small to large aromatic ring systems in chars as a function of glucose percentage in the feedstock.

4. Conclusions

This study has investigated the effect of glucose to FB ratios on N retention and migration during co-pyrolysis, with attention paid to the concurrent changes in physiochemical structures of chars. Based on the discussion above, the following conclusions can be made.

- The increase in glucose in the feedstock has significantly increased the N fixation in chars, which was a result of both enhanced volatile–char and volatile–volatile interactions with the involvement of O-containing radicals derived from the glucose devolatilizations.
- The N-containing functional groups in chars were apparently varied with the continual increase in the addition of glucose, and mainly N-5 and N-6 were identified when over 30% glucose in the feedstock was used, indicating the deep amorphous nature of volatile-derived N-O-C compounds; thus, the N species were only located at the edges of less fused aromatic rings.
- The carbon structures revealed by Raman spectroscopy for the chars derived from the co-pyrolysis at various ratios of glucose to FB were very similar, while the porous structures of chars changed obviously.

Author Contributions: Conceptualization, D.X. and S.Z.; methodology, D.X., S.Z. and L.Y.; validation, S.Z. and H.S.; formal analysis, D.X., S.Z. and L.Y.; investigation, L.Y., K. and Y.S.; resources, L.Y., K., M.Z. and Y.S.; data curation, L.Y. and M.Z.; writing—original draft preparation, S.Z. and D.X.; writing—review and editing, H.S. and X.H.; Visualization, D.X., L.Y. and S.Z.; supervision, H.S. and X.H.; project administration, H.Z. and S.Z.; funding acquisition, H.Z. and S.Z. All authors have read and agreed to the published version of the manuscript.

Funding: This research was funded by the National Natural Science Foundation of China (Grant No. 51876093); an internationally collaborative project (BRICS2019-040) under BRICS STI Framework Programme with government funding organizations of Brazil CNPq (402849/2019-1), Russia RFBR (19-58-80016), India DST (CRG/2018/004610, DST/TDT/TDP-011/2017), China MOST (2018YFE0183600), and South Africa NRF (BRIC190321424123); the Youth Innovation Fund of Nanjing Forestry University (Grant No. CX2016014).

Conflicts of Interest: The authors declare no competing financial interest.

References

1. FAOSTAT-Food and Agriculture Organistation of the United Nations. Forestry Database, Forestry Production and Trade. 2018. Available online: http://www.fao.org/faostat/en/#data/FO/visualize (accessed on 26 July 2020).
2. Ferreira, S.D.; Altafini, C.R.; Perondi, D.; Godinho, M. Pyrolysis of Medium Density Fiberboard (MDF) wastes in a screw reactor. *Energy Convers. Manag.* **2015**, *92*, 223–233. [CrossRef]
3. Xu, D.; Yang, L.; Zhao, M.; Guo, M.; Hu, X.; Gholizadeh, M.; Zhang, H.; Zhang, S. Effects of glucose on nitrogen retention and transformation during copyrolysis with fiberboard waste. *Energy Fuels* **2020**, *34*, 11083–11090. [CrossRef]
4. Zhuang, X.; Huang, Y.; Song, Y.; Zhan, H.; Yin, X.; Wu, C. The transformation pathways of nitrogen in sewage sludge during hydrothermal treatment. *Bioresour. Technol.* **2017**, *245*, 463–470. [CrossRef]
5. Huang, J.; Wang, Z.; Qiao, Y.; Wang, B.; Xu, M. Transformation of nitrogen during hydrothermal carbonization of sewage sludge: Effects of temperature and Na/Ca acetates addition. *Proc. Combust. Inst.* **2020**, in press. [CrossRef]
6. Cheng, S.; Qiao, Y.; Huang, J.; Wang, W.; Wang, Z.; Yu, Y.; Xu, M. Effects of Ca and Na acetates on nitrogen transformation during sewage sludge pyrolysis. *Proc. Combust. Inst.* **2019**, *37*, 2715–2722. [CrossRef]
7. Zhan, H.; Zhuang, X.; Song, Y.; Huang, Y.; Liu, H.; Yin, X.; Wu, C. Evolution of nitrogen functionalities in relation to NO_x precursors during low-temperature pyrolysis of biowastes. *Fuel* **2018**, *218*, 325–334. [CrossRef]
8. Li, K.; Zhang, L.; Zhu, L.; Zhu, X. Comparative study on pyrolysis of lignocellulosic and algal biomass using pyrolysis-gas chromatography/mass spectrometry. *Bioresour. Technol.* **2017**, *234*, 48–52. [CrossRef]
9. Chen, W.; Yang, H.; Chen, Y.; Chen, X.; Fang, Y.; Chen, H. Biomass pyrolysis for nitrogen-containing liquid chemicals and nitrogen-doped carbon materials. *J. Anal. Appl. Pyrol.* **2016**, *120*, 186–193. [CrossRef]
10. Mayer, F.M.; Teixeira, C.M.; Pacheco, J.G.A.; de Souza, C.T.; Bauer, D.V.; Caramão, E.B.; Espíndola, J.S.; Trierweiler, J.O.; Perez-Lopez, O.W.; Zini, C.A. Characterization of analytical fast pyrolysis vapors of Medium-Density Fiberboard (MDF) using metal-modified HZSM-5. *J. Anal. Appl. Pyrol.* **2018**, *136*, 87–95. [CrossRef]
11. Nakai, T.; Kartal, S.N.; Hata, T.; Imamura, Y. Chemical characterization of pyrolysis liquids of wood-based composites and evaluation of their bio-efficiency. *Build. Sci.* **2007**, *42*, 1236–1241. [CrossRef]
12. Chen, H.; Xie, Y.; Chen, W.; Xia, M.; Li, K.; Chen, Z.; Chen, Y.; Yang, H. Investigation on co-pyrolysis of lignocellulosic biomass and amino acids using TG-FTIR and Py-GC/MS. *Energy Convers. Manag.* **2019**, *196*, 320–329. [CrossRef]
13. Xu, D.; Gao, Y.; Lin, Z.; Gao, W.; Zhang, H.; Karnowo, K.; Hu, X.; Sun, H.; Syedhassan, S.S.A.; Zhang, S. Application of biochar derived from pyrolysis of waste fiberboard on tetracycline adsorption in aqueous solution. *Front. Chem.* **2020**, *7*, 943. [CrossRef] [PubMed]
14. Liu, J.; Deng, Y.; Li, X.; Wang, L. Promising nitrogen-rich porous carbons derived from one-step calcium chloride activation of biomass-based waste for high performance supercapacitors. *ACS Sustain.Chem. Eng.* **2016**, *4*, 177–187. [CrossRef]
15. Yuan, S.; Tan, Z.; Huang, Q. Migration and transformation mechanism of nitrogen in the biomass–biochar–plant transport process. *Renew. Sustain. Energy Rev.* **2018**, *85*, 1–13. [CrossRef]
16. Chen, W.; Fang, Y.; Li, K.; Chen, Z.; Xia, M.; Gong, M.; Chen, Y.; Yang, H.; Tu, X.; Chen, H. Bamboo wastes catalytic pyrolysis with N-doped biochar catalyst for phenols products. *Appl. Energy* **2020**, *260*, 114242. [CrossRef]

17. Leng, L.; Xu, S.; Liu, R.; Yu, T.; Zhuo, X.; Leng, S.; Xiong, Q.; Huang, H. Nitrogen containing functional groups of biochar: An overview. *Bioresour. Technol.* **2020**, *298*, 122286. [CrossRef]
18. Darvell, L.I.; Brindley, C.; Baxter, X.C.; Jones, J.M.; Williams, A. Nitrogen in biomass char and its fate during combustion: A model compound approach. *Energy Fuels* **2012**, *26*, 6482–6491. [CrossRef]
19. Liu, W.; Li, W.; Jiang, H.; Yu, H. Fates of chemical elements in biomass during its pyrolysis. *Chem. Rev.* **2017**, *117*, 6367–6398. [CrossRef]
20. Wei, F.; Cao, J.; Zhao, X.; Ren, J.; Wang, J.; Fan, X.; Wei, X. Nitrogen evolution during fast pyrolysis of sewage sludge under inert and reductive atmospheres. *Energy Fuels* **2017**, *31*, 7191–7196. [CrossRef]
21. Chen, W.; Yang, H.; Chen, Y.; Xia, M.; Chen, X.; Chen, H. Transformation of Nitrogen and evolution of N-containing species during algae pyrolysis. *Environ. Sci. Technol.* **2017**, *51*, 6570–6579. [CrossRef]
22. Zhang, X.; Zhan, H.; Yin, X.; Wu, C. Release characteristic of NO_x precursors during the pyrolysis of nitrogen-rich biomass. *J. Fuel Chem. Technol.* **2016**, *44*, 1464–1472.
23. Liu, X.; Luo, Z.; Yu, C.; Xie, G. Conversion mechanism of fuel-N during pyrolysis of biomass wastes. *Fuel* **2019**, *246*, 42–50. [CrossRef]
24. Gao, P.; Guo, D.; Liang, C.; Liu, G.; Yang, S. Nitrogen conversion during the rapid pyrolysis of raw/torrefied wheat straw. *Fuel* **2020**, *259*, 116227. [CrossRef]
25. Wei, F.; Cao, J.; Zhao, X.; Ren, J.; Gu, B.; Wei, X. Formation of aromatics and removal of nitrogen in catalytic fast pyrolysis of sewage sludge: A study of sewage sludge and model amino acids. *Fuel* **2018**, *218*, 148–154. [CrossRef]
26. Li, W.; Zhao, Y.; Yao, C.; Lu, J.; Li, R.; Wu, Y. Migration and transformation of nitrogen during hydrothermal liquefaction of penicillin sludge. *J. Supercrit. Fluids* **2020**, *157*, 104714. [CrossRef]
27. Sebestyen, Z.; Jakab, E.; Doman, A.; Bokrossy, P.; Bertoti, I.; Madarasz, J.; Laszlo, K. Thermal degradation of crab shell biomass, a nitrogen-containing carbon precursor. *J. Therm. Anal. Calorim.* **2020**, *142*, 301–308. [CrossRef]
28. Zhan, H.; Zhuang, X.; Song, Y.; Liu, J.; Li, S.; Chang, G.; Yin, X.; Wu, C.; Wang, X. A review on evolution of nitrogen-containing species during selective pyrolysis of waste wood-based panels. *Fuel* **2019**, *253*, 1214–1228. [CrossRef]
29. Becidan, M.; Skreiberg, Ø.; Hustad, J.E. NO_x and N_2O precursors (NH_3 and HCN) in pyrolysis of biomass residues. *Energy Fuels* **2007**, *21*, 1173–1180. [CrossRef]
30. Li, C.; Tan, L. Formation of NO_x and SO_x precursors during the pyrolysis of coal and biomass. Part III. Further discussion on the formation of HCN and NH_3 during pyrolysis. *Fuel* **2000**, *79*, 1899–1906. [CrossRef]
31. Zhuang, X.; Song, Y.; Wang, X.; Zhan, H.; Yin, X.; Wu, C.; Wang, P. Pyrolysis of hydrothermally pretreated biowastes: The controllability on the formation of NO_x precursors. *Chem. Eng. J.* **2020**, *393*, 124727. [CrossRef]
32. Liu, X.; Luo, Z.; Yu, C.; Jin, B.; Tu, H. Release mechanism of fuel-N into NO_x and N_2O precursors during pyrolysis of rice straw. *Energies* **2018**, *11*, 520. [CrossRef]
33. Zheng, A.; Li, L.; Tippayawong, N.; Huang, Z.; Zhao, K.; Wei, G.; Zhao, Z.; Li, H. Reducing emission of NO_x and SO_x precursors while enhancing char production from pyrolysis of sewage sludge by torrefaction pretreatment. *Energy* **2020**, *192*, 116620. [CrossRef]
34. Zhan, H.; Zhuang, X.; Song, Y.; Yin, X.; Cao, J.; Shen, Z.; Wu, C. Step pyrolysis of N-rich industrial biowastes: Regulatory mechanism of NO_x precursor formation via exploring decisive reaction pathways. *Chem. Eng. J.* **2018**, *344*, 320–331. [CrossRef]
35. Girods, P.; Dufour, A.; Rogaume, Y.; Rogaume, C.; Zoulalian, A. Comparison of gasification and pyrolysis of thermal pre-treated wood board waste. *J. Anal. Appl. Pyrol.* **2009**, *85*, 171–183. [CrossRef]
36. Girods, P.; Dufour, A.; Rogaume, Y.; Rogaume, C.; Zoulalian, A. Thermal removal of nitrogen species from wood waste containing urea formaldehyde and melamine formaldehyde resins. *J. Hazard. Mater.* **2008**, *159*, 210–221. [CrossRef]
37. Ma, Z.; Zhang, Y.; Li, C.; Yang, Y.; Zhang, W.; Zhao, C.; Wang, S. N-doping of biomass by ammonia (NH_3) torrefaction pretreatment for the production of renewable N-containing chemicals by fast pyrolysis. *Bioresour. Technol.* **2019**, *292*, 122034. [CrossRef]
38. Hulicova-Jurcakova, D.; Seredych, M.; Lu, G.; Bandosz, T.J. Combined effect of nitrogen- and oxygen-containing functional groups of microporous activated carbon on its electrochemical performance in supercapacitors. *Adv. Funct. Mater.* **2009**, *19*, 438–447. [CrossRef]

39. Hulicova-Jurcakova, D.; Seredych, M.; Lu, G.; Kodiweera, N.K.A.C.; Stallworth, P.E.; Greenbaum, S.; Bandosz, T.J. Effect of surface phosphorus functionalities of activated carbons containing oxygen and nitrogen on electrochemical capacitance. *Carbon* **2009**, *47*, 1576–1584. [CrossRef]
40. Li, Y.; Xing, B.; Wang, X.; Wang, K.; Zhu, L.; Wang, S. Nitrogen-doped hierarchical porous biochar derived from corn stalks for phenol-enhanced adsorption. *Energy Fuels* **2019**, *33*, 12459–12468. [CrossRef]
41. Chen, W.; Chen, Y.; Yang, H.; Xia, M.; Li, K.; Chen, X.; Chen, H. Co-pyrolysis of lignocellulosic biomass and microalgae: Products characteristics and interaction effect. *Bioresour. Technol.* **2017**, *245*, 860–868. [CrossRef]
42. Chen, W.; Yang, H.; Chen, Y.; Li, K.; Xia, M.; Chen, H. Influence of biochar addition on nitrogen transformation during copyrolysis of algae and lignocellulosic biomass. *Environ. Sci. Technol.* **2018**, *52*, 9514–9521. [CrossRef] [PubMed]
43. Falco, C.; Sevilla, M.; White, R.J.; Rothe, R.; Titirici, M.M. Renewable nitrogen-doped hydrothermal carbons derived from microalgae. *ChemSusChem* **2012**, *5*, 1834–1840. [CrossRef] [PubMed]
44. Jing, H.; Kitts, D.D. Chemical characterization of different sugar-casein Maillard reaction products and protective effects on chemical-induced cytotoxicity of Caco-2 cells. *Food Chem. Toxicol.* **2004**, *42*, 1833–1844. [CrossRef] [PubMed]
45. Zhang, B.; Xu, P.; Qiu, Y.; Yu, Q.; Ma, J.; Wu, H.; Luo, G.; Xu, M.; Yao, H. Increasing oxygen functional groups of activated carbon with non-thermal plasma to enhance mercury removal efficiency for flue gases. *Chem. Eng. J.* **2015**, *263*, 1–8. [CrossRef]
46. Chen, W.; Chen, Y.; Yang, H.; Li, K.; Chen, X.; Chen, H. Investigation on biomass nitrogen-enriched pyrolysis: Influence of temperature. *Bioresour. Technol.* **2018**, *249*, 247–253. [CrossRef] [PubMed]
47. Lv, D.; Xu, M.; Liu, X.; Zhan, Z.; Li, Z.; Yao, H. Effect of cellulose, lignin, alkali and alkaline earth metallic species on biomass pyrolysis and gasification. *Fuel Process. Technol.* **2010**, *91*, 903–909. [CrossRef]
48. Zhang, S.; Chen, Z.; Zhang, H.; Wang, Y.; Xu, X.; Cheng, L.; Zhang, Y. The catalytic reforming of tar from pyrolysis and gasification of brown coal: Effects of parental carbon materials on the performance of char catalysts. *Fuel Process. Technol.* **2018**, *174*, 142–148. [CrossRef]
49. Huang, Y.; Liu, S.; Wu, Y.; Zhu, X.; Xu, Z.; Li, B.; Hu, X.; Sun, H.; Zhou, J.; Zhang, S. Volatile-char interactions during biomass pyrolysis: Contribution of amino group on graphitized carbon nanotube to xylose evolution based on experimental and theoretical studies. *Fuel* **2020**, *282*, 118921. [CrossRef]
50. Zhang, S.; Min, Z.; Tay, H.L.; Asadullah, M.; Li, C.Z. Effects of volatile–char interactions on the evolution of char structure during the gasification of Victorian brown coal in steam. *Fuel* **2011**, *90*, 1529–1535. [CrossRef]
51. Wang, B.; Huang, J.; Gao, X.; Qiao, Y. Effects of Secondary Vapor-Phase Reactions on the Distribution of Chlorine Released from the Pyrolysis of KCl-Loaded Wood. *Energy Fuels* **2020**, *34*, 11717–11721. [CrossRef]
52. Hirata, T.; Kawamoto, S.; Okuro, A. Pyrolysis of melamine–formaldehyde and urea–formaldehyde resins. *J. Appl. Polym. Sci.* **1991**, *42*, 3147–3163. [CrossRef]
53. Maliutina, K.; Tahmasebi, A.; Yu, J. The transformation of nitrogen during pressurized entrained-flow pyrolysis of Chlorella vulgaris. *Bioresour. Technol.* **2018**, *262*, 90–97. [CrossRef] [PubMed]
54. Wei, L.; Wen, L.; Yang, T.; Zhang, N. Nitrogen Transformation during Sewage Sludge Pyrolysis. *Energ. Fuel.* **2015**, *29*, 5088–5094. [CrossRef]
55. Yu, W.; Lian, F.; Cui, G.; Liu, Z. N-doping effectively enhances the adsorption capacity of biochar for heavy metal ions from aqueous solution. *Chemosphere* **2018**, *193*, 8–16. [CrossRef]
56. Ding, T.; Zhao, J.; Zhu, N.; Wang, C. A comparative study of morphological characteristics of medium-density fiberboard dust by sieve and image analyses. *J. Wood Sci.* **2020**, *66*, 1–9. [CrossRef]
57. Smith, M.W.; Pecha, B.; Helms, G.; Scudiero, L.; Garciaperez, M. Chemical and morphological evaluation of chars produced from primary biomass constituents: Cellulose, xylan, and lignin. *Biomass Bioenergy* **2017**, *104*, 17–35. [CrossRef]
58. Guizani, C.; Haddad, K.; Limousy, L.; Jeguirim, M. New insights on the structural evolution of biomass char upon pyrolysis as revealed by the Raman spectroscopy and elemental analysis. *Carbon* **2017**, *119*, 519–521. [CrossRef]